

Article

Optimal Prosumer Operation with Consideration for Bounded Rationality in Peer-to-Peer Energy Trading Systems

Jianhong Hao¹, Ting Huang¹ , Yi Sun^{1,*}, Xiangpeng Zhan² , Yu Zhang³ and Peng Wu³

¹ School of Electrical and Electronic Engineering, North China Electric Power University, Beijing 102206, China; jianhonghao@ncepu.edu.cn (J.H.); huangtncepu@163.com (T.H.)

² Marketing Service Center, State Grid Fujian Electric Power Co., Ltd., Xiamen 361006, China; xiangpengzhan@whu.edu.cn

³ State Grid Energy Research Institute Co., Ltd., Beijing 100083, China; zhangyu2@sgeri.sgcc.com.cn (Y.Z.); wupeng@sgeri.sgcc.com.cn (P.W.)

* Correspondence: sy@ncepu.edu.cn

Abstract: With the large-scale development of distributed energy on the demand side, the trend of “supply exceeding demand” has gradually become prominent, and regional peer-to-peer (P2P) energy trading has become an important measure to improve the local consumption of distributed energy. However, most existing studies usually assume that prosumers behave entirely rationally with the goal of maximum benefit, which has been proved to deviate from the observed actual behaviors. Aiming at the optimal energy of prosumers participating in the P2P market, a prospect theory-based two-stage stochastic optimization model considering the bounded rationality was proposed to accurately simulate the decision-making behavior. Then, a benefit maximization model for the energy trading service provider (ETSP) was constructed considering the power flow constraint to ensure the safe operation of the system. Finally, an improved R-ADMM algorithm considering timeout was proposed to solve the above model and improve the convergence speed. The effectiveness of the proposed model and algorithm was verified via simulation.

Keywords: prosumer; prospect theory; random optimization; P2P energy trading



Citation: Hao, J.; Huang, T.; Sun, Y.; Zhan, X.; Zhang, Y.; Wu, P. Optimal Prosumer Operation with Consideration for Bounded Rationality in Peer-to-Peer Energy Trading Systems. *Energies* **2024**, *17*, 1724. <https://doi.org/10.3390/en17071724>

Academic Editor: Pavlos S. Georgilakis

Received: 1 March 2024

Revised: 14 March 2024

Accepted: 30 March 2024

Published: 3 April 2024



Copyright: © 2024 by the authors. Licensee MDPI, Basel, Switzerland. This article is an open access article distributed under the terms and conditions of the Creative Commons Attribution (CC BY) license (<https://creativecommons.org/licenses/by/4.0/>).

1. Introduction

With the substantial proliferation of intelligent control and demand-side response technology, the types and scales of distributed flexible resources, such as electric vehicles, energy storage systems (ESS), and temperature control loads have increased rapidly, and more traditional power consumers have turned into prosumers [1]. As a new entity on the demand side, prosumers have the source-load dual properties, who can participate in the regional energy transaction market more flexibly, and assist the grid to achieve peak cutting, local consumption, and carbon emissions reduction [2,3]. Therefore, how to maximize the benefits of prosumers in the regional energy market under the premise of ensuring the safety constraints is one of the challenges at present.

In order to promote regional power balance, the Grid-Wise Architecture Council (GWAC) began to develop and practice the transactive energy (TE) mechanism to carry out decentralized resource management for cluster prosumers [4]. In TE market, prosumers can trade energy with other prosumers directly through peer-to-peer (P2P) energy trading, which can reach the full resource flexibility, and improve the consumption ratio of local renewable energy [5,6]. The HELICE co-simulation framework and simulation model for transactive energy systems (SIMTES) have been proposed to demonstrate the applicability of P2P [7,8].

The existing P2P energy trading architecture can be divided into completely P2P distributed trading and centralized P2P trading with the energy trading service provider (ETSP) [9]. Completely distributed P2P energy trading architecture is usually based on the

blockchain, but the high construction and maintenance cost make it difficult to implement on a large scale [10]. Furthermore, the power flow constraints are usually ignored [11] or considered in the prosumers' optimization model [12]. Compared with completely P2P trading, the resource integration ability of EPST can greatly reduce the calculation and maintenance pressure of the grid market by clustering the local prosumers, so as to support the access of massive prosumers to the regional P2P market [13]. However, the existing studies consider the EPST as a virtual platform only for transaction matching, which directly manages the trading activities and the devices of prosumers. The centralized P2P trading struggles to protect prosumers' privacy. On the one hand, prosumers should have the right to make independent decisions, and the ETSP can act as a commercial entity and increase revenue by managing its self-building energy system. On the other hand, the global information is difficult to obtain for prosumers, which makes it unsuitable for practical application and may cause the voltage to exceed the limit, and affect the safe operation of the grid.

For the construction of the prosumers' model, the uncertainties of distributed photovoltaic (PV) output and prosumers' consumption behavior bring challenges to P2P transaction optimization. In recent research, the uncertainty processing methods mainly include stochastic optimization and robust optimization. By considering the worst scenarios, robust optimization is adopted to deal with the uncertainties of grid price, renewable energy generation, and load consumption, which focuses on optimizing the objective goal and improving stability [14,15]. To reduce the conservatism, distributionally robust optimization was proposed by merging a series of potential uncertainty distributions into a fuzzy set, which has been proved to significantly reduce the conservativeness of the results [16]. In [17], a conditional-distributionally robust optimization was proposed to consider the forecast error. However, the results still have a certain degree of conservatism, and cannot accurately simulate the influence of uncertain factors. Stochastic optimization theory was adopted in [18–20], in which the representative scenarios were selected based on the probability distribution of parameter uncertainty for optimal decision-making, with wide application in the uncertainty processing of source-load. However, decision-makers are assumed to be in a completely rational state in the above uncertainty processing methods, which fail to consider the risk preference of decision-makers. The psychological expectation and subjective risk preference of decision-makers are the important factors affecting the decision result. Though a risk-loss model that introduced risk weights to quantify the risk cost was constructed in [21,22], it still suffered from a lack of consideration of the tendencies and could not reflect the different subjective preferences of decision-makers under different objective probability events, which is also referred to as bounded rational behavior. The decision-makers' subjective bounded rationality is an important research branch in psychology, which represents the irrational behavior caused by the psychological activities in different scenes. Therefore, the actual choices are excluded from the objective decisions. Considering this idea, Kahneman proposed the prospect theory (PT) to reveal the irrational psychological factors affecting the selection behavior from the psychological characteristics and behavioral characteristics. This indicated the characteristics of loss avoidance and risk preference, which refers to the fact that low-probability events will be overestimated and high-probability events will be underestimated [23]. Based on the theory, the decision weight model was proposed to quantify the irrational psychological factors affecting behavioral decision-making and to describe different risk preference facing gains and losses, which verified that the proposed model is more consistent with actual behavior. In addition, as a nonlinear model, how to deal with the nonlinearity of the PT is a difficult problem to be solved in the application.

In terms of solving algorithms, it is mainly divided into centralized and distributed algorithms. Traditional centralized optimization scheduling has defects such as massive communication data, weak privacy, dimension disaster, and so on. Furthermore, with the increase in entities, it also brings challenges to the computing and maintenance capabilities of centralized platforms [24]. In terms of distributed algorithms represented

by deep reinforced learning, the energy optimal model is generally formulated as a partially observable Markov decision process [25], and then the multicluster deep reinforced learning algorithm with decentralized training structure is proposed to coordinate the management of large-scale P2P energy trading [26]. However, the aforementioned reinforcement learning algorithm requires large interaction and trial between the agent and the environment in order to collect feedback signals to learn, which makes its generalization ability weak and limits its application in costly real scenarios. Therefore, the alternating direction method of multiplier (ADMM) technique has gradually become widely applied for solving models [27,28]. In [29], the ADMM algorithm was designed to manage heating, ventilation, and air-conditioning units to protect privacy. To avoid the nonconvexity caused by binary variables, the noncomplementary charging/discharging mechanism was adopted in ADMM to linearize the model [30]. However, the existing research assumed that the communication environment is ideal among prosumers. If the calculation of a single agent failure or the communication delay is large, the single iteration will be stopped, and the iterative process of the whole algorithm will be blocked, resulting in a long convergence time [31,32]. Therefore, how to guarantee the reliable convergence of the algorithm in the nonideal communication is also an urgent problem to be solved.

To sum up, although the research about P2P energy trading has developed rapidly, there are still the following challenges: (1) the security constraints of global trends are ignored; (2) lack of consideration of the bounded rationality of prosumers, which cannot accurately simulate the actual behavior; (3) the stagnant or slow convergence due to the iteration delay timeout. To solve the above problems, the main contributions of this paper can be summarized as follows:

- (1) A P2P energy trading architecture considering the ETSP with self-building energy system was proposed, and the model of ETSP was constructed considering global power flow constraints to maximize the benefit and ensure the voltage safety.
- (2) Based on prospect theory, a two-stage stochastic optimization model of prosumers considering the source-load uncertainty was constructed under bounded rationality, so as to describe the risk decision behavior more accurately.
- (3) An improved R-ADMM algorithm considering iteration delay was proposed to improve the convergence speed, and the effectiveness was verified via simulation.

2. P2P Energy Trading Architecture

The P2P energy trading architecture in the local prosumers' community is shown in Figure 1. Each prosumer consists of PV, ESS, rigid and flexible load, and an energy management system (EMS). Based on information and communication technology, prosumers can obtain the self-energy information to solve the optimal energy dispatching strategy. As the only energy service provider in the community, ETSP is responsible for the centralized coordination of regional P2P market transactions and settlements, while improving the grid operation safety and economic benefits by regulating its self-building resources. It is worth mentioning that the prosumers can only trade with other prosumers and the ETSP.

By sharing purchasing and selling power and price, the prosumers and the ETSP iteratively solve the optimal scheduling strategies satisfying the constraint conditions, until the result meets the convergence condition.

Table 1 shows the comparison of characteristics and performance evaluation indicators among the completely P2P distributed trading architecture, the centralized P2P trading architecture with ETSP and the proposed architecture. Due to the fact that the energy optimizations of the prosumer cannot be directly controlled by ETSP, the proposed framework cannot maximize the global benefit, but its performance is still the best overall.

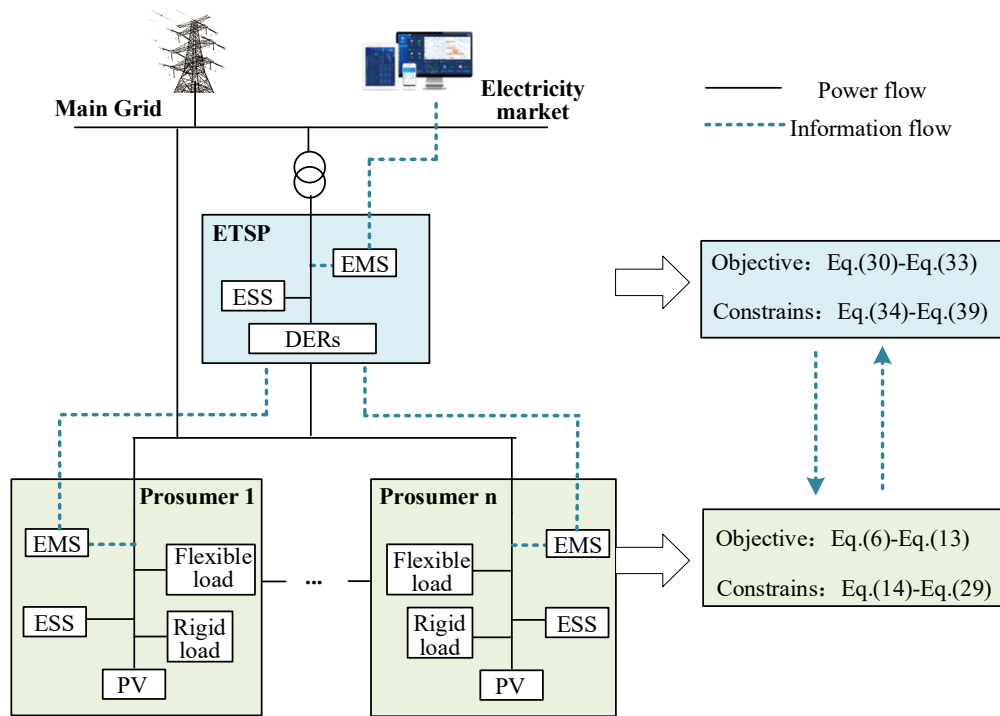


Figure 1. P2P energy trading architecture in prosumers' community.

Table 1. Analysis of three architecture of P2P energy trading.

	Features	Completely Free to Trade	High Market Efficiency	Preserve Privacy	Power Security	Benefit Maximization
Completely P2P distributed trading architecture	Negotiate without the involvement of a third party.	✓	×	✓	×	×
Centralized P2P trading architecture with ETSP	ETSP directly manages the trading activities and the devices.	×	✓	×	✓	✓
Proposed architecture	ETSP coordinates the trading activities inside the community.	✓	✓	✓	✓	×

3. Energy Optimization Model of Prosumers Considering Bounded Rationality

3.1. Prospect Theory

PT is a risk decision theory proposed by Kehneman on the basis of expected utility theory, which is used to describe the decision-making process of decision-makers in response to risks and uncertain conditions. Through a series of experimental observations, prospect theory claims that decision-making behavior is the result under bounded rationality of decision-makers, and the decision result depends on the gap between the result and the expectation rather than the result itself. When making decisions, individuals usually overestimate small probability events and underestimate large probability events. Therefore, prospect theory transforms the objective probability of events into a subjective weight to describe the individual bounded rationality behavior under psychological influence [33].

In reference [34], the subjective can be divided into value function and weight function introducing the prospect theory:

$$V_{\omega,i} = \begin{cases} (\Delta C_{\omega,i})^{\alpha_i}, & \Delta C_{\omega,i} \geq 0 \\ -\lambda_i(-\Delta C_{\omega,i})^{\beta_i}, & \Delta C_{\omega,i} < 0 \end{cases} \quad (1)$$

$$TDVF_{\omega,i} = V_{\omega,i} \delta_i (1 - (1 - \theta_i) r_i)^{1/(1-\theta_i)} \quad (2)$$

$$\Delta C_{\omega,i} = C_{\omega,i} - \bar{C}_i \quad (3)$$

where, $TDVF_{\omega,i}$ is the value function introducing risk preference based on the traditional value function, $\Delta C_{\omega,i}$ is the difference between the actual benefit $C_{\omega,i}$ and the expected benefit \bar{C}_i of the prosumer i in the scenario ω , α_i is the risk preference coefficient, β_i is the risk avoidance coefficient, λ_i is the loss avoidance coefficient representing the individual's aversion to loss, which need to be satisfied $\beta_i < 0, \alpha_i \leq 1, \lambda_i \geq 1$. δ_i is the deviation coefficient, θ_i is the double curvature coefficient, and r_i is the proportion coefficient.

Its decision weight function is shown as follows:

$$\pi_{\omega,i} = \exp(-(\ln \rho_{\omega})^{\xi_i}), \quad 0 \leq \xi_i \leq 1 \quad (4)$$

where $\pi_{\omega,i}$ is the subjective decision weight, ρ_{ω} is the true objective probability of the gain/loss event, ξ_i is the decision weight function coefficient.

Therefore, the utility function based on prospect theory is as follows:

$$R_i = \sum_{\omega=1}^{N_{\omega}} \sum_{i=1}^{N_i} \pi_{\omega,i} TDVF_{\omega,i} \quad (5)$$

3.2. Two-Stage Stochastic Optimization Model Based on PT of Prosumers

In the actual scenario, the distributed PV output has randomness, fluctuation, and intermittency. The energy consumption changes frequently and fluctuates greatly over a long time scale. The deterministic model does not take these uncertainties into account in the optimization of the total cost of the system, which results in a large deviation from the actual results. Therefore, a two-stage stochastic optimization model was constructed to realize the uncertainty optimization.

The multiscenario method was adopted to deal with the uncertainty of PV output and energy consumption, and the uncertainty factors in the model were transformed into multiple deterministic scenarios by simulating the possible scenarios. Firstly, the Monte Carlo sampling method was applied to generate a large number of scenarios to simulate the possible running states of random variables in periods. Then considering the long calculation time when solving all scenarios, this section adopted the fast forward selection method to reduce the scenes, and constructed the typical scenes and corresponding probabilities to characterize the characteristics of random scenes and reduce the calculation burden.

In the traditional stochastic optimization, the estimated probability of each scenario is usually solved by equal probability distribution or improved fast previous generation elimination technique [19]. However, it is difficult to accurately describe the bounded rationality of prosumers, which will result in the deviations in the simulation of their decision behaviors. Therefore, this section introduces the prospect theory on the basis of the traditional stochastic optimization model, and converted the objective probability into the subjective decision weight function of prosumers. Based on the N_{ω} typical scenarios through scene reduction in the traditional stochastic optimization model, the PT was adopted to calculate the subjective decision weight $\pi_{\omega,i}$ and the value function $TDVF_{\omega,i}$ in each day-in scenario, then the optimal day-ahead schedule decision was obtained under the bounded rationality when the day-in prospect reached the maximum.

The energy management optimization model considering uncertainty includes two stages: day-ahead cost C_i^{DA} and day-in prospect U_i^{RT} , aiming to minimize day-ahead

energy management cost and maximize day-in prospect, as shown in Equations (6)–(13). It is worth noting that the day-in prospect model is a nonlinear model, and its linearization transformation process is appended in the Appendix A.

$$\min C_i = C_i^{DA} - U_i^{RT} \quad (6)$$

$$C_i^{DA} = \sum_{t=1}^T \Delta t (C_{i,t}^{ET} + C_{i,t}^{SF} + C_{i,t}^L + C_{i,t}^{BY}) \quad (7)$$

$$C_{i,t}^{ET} = s_t^E \cdot P_{i,t}^{b,E} - s_t^i \cdot P_{i,t}^{s,E} + \sum_{j=1, j \neq i}^{N_i} (s_t^j \cdot P_{i,t}^{b,ij} - s_t^i \cdot P_{i,t}^{s,ij}) \quad (8)$$

$$C_{i,t}^{SF} = c_{pv} \cdot P_{i,t}^{pv} + c_{ess} \cdot (P_{i,t}^{ch} + P_{i,t}^{dch}) \quad (9)$$

$$C_{i,t}^L = c_L \cdot (P_{i,t}^R + P_{i,t}^F - P_{i,t}^{pre})^2 \quad (10)$$

$$C_{i,t}^{BY} = c_{ess}^+ (P_{i,t}^{ch+} + P_{i,t}^{dch+}) + c_{ess}^- (P_{i,t}^{ch-} + P_{i,t}^{dch-}) + c_{dr}^+ P_{i,t}^{F+} + c_{dr}^- P_{i,t}^{F-} \quad (11)$$

$$U_i^{RT} = \sum_{\omega=1}^{N_\omega} \pi_{\omega,i} TDVF_{\omega,i} \quad (12)$$

$$= \begin{cases} (\Delta U_{\omega,i})^{\alpha_i} \delta_i (1 - (1 - \theta_i) r_i)^{1/(1-\theta_i)}, & \Delta U_{\omega,i} \geq 0 \\ -\lambda_i (-\Delta U_{\omega,i})^{\beta_i} \delta_i (1 - (1 - \theta_i) r_i)^{1/(1-\theta_i)}, & \Delta U_{\omega,i} < 0 \end{cases}$$

$$\begin{cases} U_{\omega,i} = - \sum_{t=1}^T (c_{r,ess} (\Delta P_{\omega,i,t}^{ch} + \Delta P_{\omega,i,t}^{dch}) + c_{r,L} \Delta P_{\omega,i,t}^F + c_{r,pl} (\Delta P_{\omega,i,t}^{BE} + \Delta P_{\omega,i,t}^{SE})) \\ \bar{U}_{\omega,i} = - \sum_{t=1}^T (c_{r,ess} (\Delta \bar{P}_{\omega,i,t}^{ch} + \Delta \bar{P}_{\omega,i,t}^{dch}) + c_{r,L} \Delta \bar{P}_{\omega,i,t}^F + c_{r,pl} (\Delta \bar{P}_{\omega,i,t}^{BE} + \Delta \bar{P}_{\omega,i,t}^{SE})) \\ \Delta U_{\omega,i} = U_{\omega,i} - \bar{U}_{\omega,i} \end{cases} \quad (13)$$

where, $U_{\omega,i}$ is the day-in expected income, $\bar{U}_{\omega,i}$ is the day-in reference income, and $\Delta U_{\omega,i}$ is the difference between the day-in expected income and reference income. Δt is the time interval. $C_{i,t}^{ET}$, $C_{i,t}^{SF}$, and $C_{i,t}^L$ are the energy transaction costs, operation and maintenance costs, and comfort loss costs of the prosumer i . $P_{i,t}^{b,E}$ and $P_{i,t}^{s,E}$ are the purchasing and selling power by prosumer i from ETSP, respectively. $P_{i,t}^{b,ij}$ and $P_{i,t}^{s,ij}$ are the purchasing and selling power of prosumer i from prosumer j respectively. $s_t^{E,i}$ is the selling price of the ETSP to the prosumer i , and s_t^i is the selling price of the prosumer i to others. $P_{i,t}^{pv}$ refers to the PV output of prosumer i during the period t , $P_{i,t}^{ch}$ and $P_{i,t}^{dch}$ are the charging and discharging power of ESS respectively. $P_{i,t}^F$ is the flexible load, $P_{i,t}^R$ is the rigid load, and $P_{i,t}^{pre}$ is the predicted power consumption. $P_{i,t}^{ch+}$, $P_{i,t}^{ch-}$, $P_{i,t}^{dch+}$, $P_{i,t}^{dch-}$ are respectively the upstream reserve and downstream reserve for charging and discharging of ESS, $P_{i,t}^{F+}$ and $P_{i,t}^{F-}$ are the upstream reserve and downstream reserve for adjusting the flexible load. c_{ess}^+ , c_{ess}^- , c_{dr}^+ and c_{dr}^- are the corresponding unit reserve costs respectively. $\Delta P_{\omega,i,t}^{ch}$, $\Delta P_{\omega,i,t}^{dch}$, $\Delta P_{\omega,i,t}^F$, $\Delta P_{\omega,i,t}^{BE}$, $\Delta P_{\omega,i,t}^{SE}$ are the adjustment power of charge and discharge of ESS, flexible load and power purchased/sold to ETSP in the day-in scheduling in scenario ω . $\Delta \bar{P}_{\omega,i,t}^{ch}$, $\Delta \bar{P}_{\omega,i,t}^{dch}$, $\Delta \bar{P}_{\omega,i,t}^F$, $\Delta \bar{P}_{\omega,i,t}^{BE}$, $\Delta \bar{P}_{\omega,i,t}^{SE}$ are the corresponding expected adjustment amount solved based on historical data, where the positive values represent upward adjustment and negative values downward adjustment. c_{pv} , c_{ess} , c_L are the adjustment cost coefficients of PV, ESS, flexible load respectively. $c_{r,ess}$, $c_{r,L}$, $c_{r,pl}$ are the day-in unit adjustment costs of ESS, flexible load and purchased power respectively.

3.3. Day-Ahead Constraints

(1) Power demand constraints

$$\underline{D}_i \leq \sum_{t=1}^T \Delta t \cdot (P_{i,t}^R + P_{i,t}^F - P_{i,t}^{F+} + P_{i,t}^{F-}) \leq \overline{D}_i \quad (14)$$

$$\underline{d}_{i,t} \leq (P_{i,t}^R + P_{i,t}^F - P_{i,t}^{F+} + P_{i,t}^{F-}) \leq \overline{d}_{i,t} \quad (15)$$

\underline{D}_i and \overline{D}_i are the minimum and maximum of the total power after adjustment within the period, $\underline{d}_{i,t}$ and $\overline{d}_{i,t}$ are the minimum and maximum of the power after adjustment within a time slot.

(2) ESS constraints

Assuming that the ESS is dominated by batteries, the charge and discharge constraints should be met as follows:

$$\begin{cases} 0 \leq P_{i,t}^{ch} - P_{i,t}^{ch+} + P_{i,t}^{ch-} \leq \overline{P}_i^{ch} \\ 0 \leq P_{i,t}^{dch} + P_{i,t}^{dch+} - P_{i,t}^{dch-} \leq \overline{P}_i^{dch} \\ P_{i,t}^{ch} \cdot P_{i,t}^{dch} = 0 \end{cases} \quad (16)$$

$$E_{i,t} = E_{i,t-1} + \eta_i^{ch} \cdot P_{i,t}^{ch} \cdot \Delta t - P_{i,t}^{dch} \cdot \Delta t / \eta_i^{dch} \quad (17)$$

$$E_i^{\min} \leq E_{i,t} \leq E_i^{\max} \quad (18)$$

The ESS can only charge or discharge in the same period, \overline{P}_i^{ch} and \overline{P}_i^{dch} are the maximum charge and discharge power in the period t , respectively. η_i^{ch} and η_i^{dch} are the charging and discharging coefficients, respectively, and $E_{i,t}$ is the energy capacity at time t . E_i^{\min} and E_i^{\max} are the maximum and minimum of the ESS capacity.

The nonlinear constraint in Formula (16) is transformed into a linear constraint by the big-M method as follows, $\mu_{i,t}^{ess}$ represents the charge and discharge state of the energy storage, which is a binary variable, and M is assumed to be an infinite constant.

$$\begin{cases} \mu_{i,t}^{ess} \leq P_{i,t}^{ch} \leq M \mu_{i,t}^{ess} \\ (1 - \mu_{i,t}^{ess}) \leq P_{i,t}^{dch} \leq M(1 - \mu_{i,t}^{ess}) \end{cases} \quad (19)$$

(3) Purchase and sale power constraints

$$\begin{cases} 0 \leq P_{i,t}^{b,E} \leq \overline{P}_{i,t}^{b,E} \\ 0 \leq P_{i,t}^{s,E} \leq \overline{P}_{i,t}^{s,E} \end{cases} \quad (20)$$

$$\begin{cases} 0 \leq P_{i,t}^{b,ij} \leq \overline{P}_{i,t}^{b,ij}, j = 1, 2, \dots, N_i, j \neq i \\ 0 \leq P_{i,t}^{s,ij} \leq \overline{P}_{i,t}^{s,ij}, j = 1, 2, \dots, N_i, j \neq i \end{cases} \quad (21)$$

where $\overline{P}_{i,t}^{b,E}$ and $\overline{P}_{i,t}^{s,E}$ are the maximum purchasing and selling power of prosumer i from ETSP, $\overline{P}_{i,t}^{b,ij}$ and $\overline{P}_{i,t}^{s,ij}$ are the maximum purchasing and selling power by prosumer i from prosumer j .

Considering that prosumer i can only participate in the market as a buyer or seller in the same period of time, the following constraints must also be met:

$$[P_{i,t}^{b,E}, P_{i,t}^{b,i1}, \dots, P_{i,t}^{b,iN}]^T \cdot [P_{i,t}^{s,E}, P_{i,t}^{s,i1}, \dots, P_{i,t}^{s,iN}] = 0 \quad (22)$$

(4) Power balance constraints

Following the principle of conservation of energy, prosumers should meet the following power balance constraints:

$$P_{i,t}^R + P_{i,t}^F + P_{i,t}^{ch} + P_{i,t}^{s,E} + \sum_{j=1, j \neq i}^N P_{i,t}^{s,ij} = P_{i,t}^{pv} + P_{i,t}^{dch} + P_{i,t}^{b,E} + \sum_{j=1, j \neq i}^N P_{i,t}^{b,ij} \quad (23)$$

3.4. Day-In Constraints

In day-in scheduling, prosumers adjust the ESS, load and purchasing and selling power according to the actual PV output and energy demand. The specific constraints are as follows:

$$\Delta P_{\omega,i,t}^F + P_{i,t}^F + P_{i,t}^{R*} + \Delta P_{\omega,i,t}^{ch} + P_{i,t}^{ch} + \Delta P_{\omega,i,t}^{s,E} + P_{i,t}^{s,E} + \sum_{j=1, j \neq i}^N P_{i,t}^{s,ij} = P_{i,t}^{pv*} + \Delta \bar{P}_{\omega,i,t}^{dch} + P_{i,t}^{dch} + \Delta P_{\omega,i,t}^{b,E} + P_{i,t}^{b,E} + \sum_{j=1, j \neq i}^N P_{i,t}^{b,ij} \quad (24)$$

$$\begin{cases} -M\mu_{i,t}^{ess} \leq \Delta P_{\omega,i,t}^{ch} \leq M\mu_{i,t}^{ess} \\ -P_{i,t}^{ch+} \leq \Delta P_{\omega,i,t}^{ch} \leq P_{i,t}^{ch-} \end{cases} \quad (25)$$

$$\begin{cases} -M(1 - \mu_{i,t}^{ess}) \leq \Delta P_{\omega,i,t}^{dch} \leq M(1 - \mu_{i,t}^{ess}) \\ -P_{i,t}^{dch-} \leq \Delta P_{\omega,i,t}^{dch} \leq P_{i,t}^{dch+} \end{cases} \quad (26)$$

$$\begin{cases} -M\mu_{i,t}^{BS} \leq \Delta P_{\omega,i,t}^{s,E} \leq M\mu_{i,t}^{BS} \\ 0 \leq P_{i,t}^{s,E} + \Delta P_{\omega,i,t}^{s,E} \leq \bar{P}_{i,t}^{s,E} \end{cases} \quad (27)$$

$$\begin{cases} -M(1 - \mu_{i,t}^{BS}) \leq \Delta P_{\omega,i,t}^{b,E} \leq M(1 - \mu_{i,t}^{BS}) \\ 0 \leq P_{i,t}^{b,E} + \Delta P_{\omega,i,t}^{b,E} \leq \bar{P}_{i,t}^{b,E} \end{cases} \quad (28)$$

$$\begin{cases} \underline{D}_i \leq \sum_{t=1}^T \Delta t \cdot (P_{i,t}^F + P_{i,t}^{R*} + \Delta P_{\omega,i,t}^F) \leq \bar{D}_i \\ -P_{i,t}^{F+} \leq \Delta P_{\omega,i,t}^F \leq P_{i,t}^{F-} \end{cases} \quad (29)$$

where, Equation (24) refers to the day-in real-time power balance constraint, Equations (25) and (26) refer to the charge and discharge constraints of ESS (the charge and discharge state of the two stages should be consistent), and Equations (27) and (28) refer to the purchasing and selling power constraints (the purchasing/selling role of the prosumer in the two stages should be consistent). Equation (29) is the load adjustment constraint. $P_{i,t}^{R*}$ and $P_{i,t}^{pv*}$ refer to the actual rigid load demand and PV output, and $\mu_{i,t}^{BS}$ refers to the role of purchasing/selling role of prosumer i in the day-ahead, where 0 represents the selling and 1 represents the purchasing.

4. Benefit Maximization Model of ETSP Considering Power Flow Constraints

Assuming that ETSP builds its own controllable distributed generation and ESS, it can purchase and sell power with the grid, and also trade power with other prosumers. The objective function is to minimize the daily operating cost including the energy transaction cost and the operating cost of the self-building energy system, as shown in Equations (30)–(33).

$$\min C_E = \sum_{t=1}^T \Delta t (C_{E,t}^{ET} + C_{E,t}^{MG} + C_{E,t}^{SF}) \quad (30)$$

$$C_{E,t}^{ET} = \sum_{i=1}^{N_i} s_t^i \cdot P_{i,t}^{s,E} - s_t^E \cdot P_{i,t}^{b,E} \quad (31)$$

$$C_{E,t}^{MG} = b_t^g \cdot P_{E,t}^{g^b} - s_t^g \cdot P_{E,t}^{g^s} \quad (32)$$

$$C_{E,t}^{SF} = c_{gt} \cdot P_{E,t}^{gt} + c_{ess} \cdot (P_{E,t}^{ch} + P_{E,t}^{dch}) \tag{33}$$

where, s_t^g and b_t^g are selling and purchasing price of the grid, $P_{E,t}^{gb}$ and $P_{E,t}^{gs}$ are the purchasing and selling power of the ETSP from the grid respectively. $P_{E,t}^{gt}$ is the generation power of the self-built controllable distributed generation, $P_{E,t}^{ch}$ and $P_{E,t}^{dch}$ are the charge and discharge power of ESS, c_{gt} is the power generation cost coefficient of controllable distributed generation.

- (1) ESS constraints Refer to the ESS constraints of prosumers.
- (2) Purchase and sale power constraints ETSP can only participate in the grid market as a buyer or seller at the same time.

$$\begin{cases} 0 \leq P_{E,t}^{gb} \leq \bar{P}_{E,t}^{gb} \\ 0 \leq P_{E,t}^{gs} \leq \bar{P}_{E,t}^{gs} \\ P_{E,t}^{gb} \cdot P_{E,t}^{gs} = 0 \end{cases} \tag{34}$$

$\underline{P}_{E,t}^{gt}$ and $\bar{P}_{E,t}^{gt}$ are the maximum purchasing and selling power of EPST from the grid. It is worth noting that the nonlinear constraint in Equation (34) can be linearized via the big-M method, which has been shown in Equation (20) and not be further described here.

- (3) Controllable distributed generation constraints

Micro-gas turbine is taken as the main controllable distributed generation, and its power response speed is faster than that of hour-level scheduling. Therefore, its climb rate constraint can be ignored, but the output power constraint should be satisfied:

$$\underline{P}_{E,t}^{gt} \leq P_{E,t}^{gt} \leq \bar{P}_{E,t}^{gt} \tag{35}$$

$\underline{P}_{E,t}^{gt}$ and $\bar{P}_{E,t}^{gt}$ are the minimum and maximum output of the distributed generation.

- (4) Power flow constraint

Using the power flow constraint linearization method proposed in [35], the linearized power flow function between node voltage and injected power can be obtained:

$$\begin{bmatrix} \mathbf{U}_{re}^t \\ \mathbf{U}_{im}^t \end{bmatrix} = \begin{bmatrix} \mathbf{Y}_{re} & -\mathbf{Y}_{im} \\ -\mathbf{Y}_{im} & -\mathbf{Y}_{re} \end{bmatrix}^{-1} \begin{bmatrix} \mathbf{P}^t \\ \mathbf{Q}^t \end{bmatrix} = \begin{bmatrix} \mathbf{R} & \mathbf{X} \\ \mathbf{X} & -\mathbf{R} \end{bmatrix} \begin{bmatrix} \mathbf{P}^t \\ \mathbf{Q}^t \end{bmatrix} \tag{36}$$

where, $\mathbf{Y}_{re} = \text{Re}(\mathbf{Y})$ and $\mathbf{Y}_{im} = \text{Im}(\mathbf{Y})$ are the real and imaginary parts of the node admittance matrix respectively, \mathbf{P}^t and \mathbf{Q}^t are the active and reactive power vectors injected by the node respectively; \mathbf{R} and \mathbf{X} are the real and imaginary parts of the modified node impedance matrix respectively.

Therefore, the node voltage amplitude and phase angle can be approximated as $|\mathbf{U}| = \mathbf{U}_{re}$, $\theta = \mathbf{U}_{im}$.

To ensure the safe operation of the distribution network and avoid line overload, the following voltage constraints and line capacity constraints should be met:

$$\underline{\mathbf{U}} \leq \mathbf{U}_{re}^t = \mathbf{R}\mathbf{P}^t + \mathbf{X}\mathbf{Q}^t \leq \bar{\mathbf{U}} \tag{37}$$

$$\underline{\mathbf{I}} \leq \mathbf{I}^t = \mathbf{L}\mathbf{A}\mathbf{U}_{re}^t = \mathbf{L}\mathbf{A}(\mathbf{R}\mathbf{P}^t + \mathbf{X}\mathbf{Q}^t) \leq \bar{\mathbf{I}} \tag{38}$$

where, \mathbf{A} is the node branch association matrix of dimension $m \times n$. m and n are the number of branches and the number of nodes respectively. \mathbf{L} is an M -order diagonal matrix

composed of absolute value of branch admittance. $\bar{\mathbf{U}}$ and $\underline{\mathbf{U}}$ are the upper and lower limits of the branch voltage. $\bar{\mathbf{I}}$ and $\underline{\mathbf{I}}$ are the upper and lower limits of the branch current.

(5) Power balance constraints

$$P_{E,t}^{gt} + P_{E,t}^{dch} + P_{E,t}^{gs} + \sum_{i=1}^{N_i} P_{i,t}^{s,E} = P_{E,t}^{ch} + P_{E,t}^{gb} + \sum_{i=1}^{N_i} P_{i,t}^{s,E} \tag{39}$$

5. Solution Algorithm

5.1. Relaxed ADMM (R-ADMM)

In view of the above optimization problems, this section first describes them as global optimization problems:

$$\begin{cases} \min C_{ETSP}(x_E, v_E) + \sum_{i \in N} C_{P,i}(x_{P,i}, v_{P,i}) \\ \text{s.t. } G_{P,i}(x_{P,i}, v_{P,i}) \leq 0, H_{P,i}(x_{P,i}, v_{P,i}) = 0 \\ G_{ETSP}(x_E, v_E) \leq 0, H_{ETSP}(x_E, v_E) = 0 \\ v_{P,i} - v_{E,i} = 0 \end{cases} \tag{40}$$

where, $x_{P,i}$ and x_E are the independent decision variables of prosumer i and ETSP in their respective optimization problems respectively, $v_{P,i}$ and v_E are the coupled variables, $v_{E,i}$ is the coupled variables of ETSP corresponding to prosumer i , and the corresponding coupled variables of each subject should be equal. $G(\cdot)$ and $H(\cdot)$ represent the above inequality constraints and equality constraints.

Based on the standard ADMM algorithm, the above original problems were decomposed into multiple subproblems that can be solved independently within each subject to ensure the data privacy. To further improve the algorithm convergence, an improved R-ADMM based on Peaceman-Rachford (P-R) splitting method was introduced [31], and its optimization subproblem can be transformed into the following form:

$$\hat{v}_{P,i,k+1} = \operatorname{argmin} C_{P,i}(x_{P,i}, v_{P,i,k}) + (z_{P,i,k})^T v_{P,i,k} + \frac{\rho}{2} \|v_{P,i,k}\|_2^2 \tag{41}$$

$$\hat{v}_{E,i,k+1} = \operatorname{argmin} C_{E,i}(x_{P,i}, v_{E,i,k}) + (z_{E,i,k})^T v_{E,i,k} + \frac{\rho}{2} \|v_{E,i,k}\|_2^2 \tag{42}$$

where $\hat{v}_{P,i,k+1}$ and $\hat{v}_{E,i,k+1}$ are the coupling variable corresponding to the prosumer i and ETSP. ρ is the quadratic penalty coefficient, $z_{P,i,k}$ and $z_{E,i,k}$ are the Lagrange multiplier, which are updated according to Equation (43):

$$\begin{cases} z_{P,i,k+1} = (\alpha - 1)z_{P,i,k} + \alpha q_{i,k+1}^{E \rightarrow P} \\ z_{E,i,k+1} = (\alpha - 1)z_{E,i,k} + \alpha q_{i,k+1}^{P \rightarrow E} \end{cases} \tag{43}$$

where α is the relaxation factor, and when its value is 0.5, R-ADMM and standard ADMM are equivalent. $q_{i,k+1}^{E \rightarrow P}$ represents the boundary variable passed by ETSP to prosumer i , and $q_{i,k+1}^{P \rightarrow E}$ represents the boundary variable passed by prosumer i to ETSP. The $q_{i,k}^{E \rightarrow P}$ and $q_{i,k}^{P \rightarrow E}$ is calculated as follows:

$$\begin{cases} q_{i,k+1}^{E \rightarrow P} = z_{E,i,k+1} - 2\rho \hat{v}_{E,i,k+1} \\ q_{i,k+1}^{P \rightarrow E} = z_{P,i,k+1} - 2\rho \hat{v}_{P,i,k+1} \end{cases} \tag{44}$$

When the error between the coupled variables is less than the allowed value ε as shown in the (45), the result can be considered to have reached convergence:

$$\left\| \hat{v}_{P,i,k+1} - \hat{v}_{E,i,k+1} \right\|_2 \leq \varepsilon \tag{45}$$

According to [31,32], the convergence of R-ADMM can be guaranteed.

5.2. Improved R-ADMM Algorithm Considering Iteration Timeout

In the above iteration process, R-ADMM still performs the calculation in serial mode, which means that ETSP needs to receive the updated boundary variables from each prosumer to start the next iteration. However, if the calculation timeout or communication timeout occurs in prosumer i , ETSP cannot receive the updated boundary variable of this iteration in a short time, and then cannot update the Lagrange multiplier, which will result in the algorithm stagnation and affect the convergence speed. To solve this problem, an improved R-ADMM algorithm considering iteration delay was proposed in this section. The transfer factor was introduced to determine whether the boundary variable was successfully passed, and momentum extrapolation prediction was proposed to correct the boundary variable that fails to be transmitted, so as to deal with the iteration timeout and accelerate the algorithm convergence speed.

This section first defines the binary variable $o_{P,i,k}$ as transfer factors, and determined whether the boundary variables of prosumer i failed to transmit in the k th iteration by judging whether the iteration time reached the tolerance time t_{THR} :

$$\begin{cases} o_{P,i,k} = 1 & \text{if } t_{P,i,k} > t_{THR} \\ o_{P,i,k} = 0 & \text{if } t_{P,i,k} \leq t_{THR} \end{cases} \quad (46)$$

$t_{P,i,k}$ is the total time of calculation time and communication delay of the k th iteration of prosumer i .

The variable correction mechanism is shown as follows.

- (1) If $o_{P,i,k}$ is 0 which means that prosumer i successfully transmits the boundary variables to ETSP within the tolerance time in the k th iteration, and then ETSP updates normally according to Equation (44);
- (2) If $o_{P,i,k}$ is 1 which means that prosumer i fails to transmit the boundary variables to ETSP within the tolerance time in the k th iteration. At this time, ETSP cannot update the multiplier $z_{E,i,k}$ without receiving the boundary variables $q_{i,k+1}^{P \rightarrow E}$ and keeps the result of the last iteration. Similarly, when iteration timeout occurs on ETSP, prosumer i cannot receive the boundary information $q_{i,k+1}^{E \rightarrow P}$ from ETSP, and cannot further update the corresponding Lagrange multiplier $z_{P,i,k}$. At this time, the momentum extrapolation prediction correction mechanism was introduced to predict the boundary information in this iteration, and then the predicted value is brought into Equation (47) to correct and update the Lagrange multiplier to accelerate the convergence speed. The momentum extrapolation prediction correction mechanism is shown as follows:

$$\begin{cases} m_{i,k}^{P \rightarrow E} = \kappa^M m_{i,k-1}^{P \rightarrow E} + \kappa^E (\tilde{q}_{i,k}^{P \rightarrow E} - \tilde{q}_{i,k-1}^{P \rightarrow E}) \\ \tilde{q}_{i,k+1}^{P \rightarrow E} = \tilde{q}_{i,k}^{P \rightarrow E} + m_{i,k}^{P \rightarrow E} \end{cases} \quad (47)$$

where, $m_{i,k}^{P \rightarrow E}$ is the momentum term, $(\tilde{q}_{i,k}^{P \rightarrow E} - \tilde{q}_{i,k-1}^{P \rightarrow E})$ is the linear extrapolation term, κ^M and κ^E are the corresponding extrapolation coefficients.

Similarly, when iteration timeout occurs on ETSP, prosumers also use the above mechanism to forecast and update the Lagrange multiplier.

6. Discussion

6.1. Simulation Setup

In order to verify the effectiveness of the proposed algorithm, this paper adopted standard IEEE33 nodes for simulation. The system was equipped with five prosumers. The PV output, load data and ESS parameters were derived from [11,36]. The 200 scenarios of PV output and load were generated, and five typical scenarios were formed through scene reduction, which are shown in Appendix B. The day-ahead selling price to the grid was 0.4 RMB/kWh, and the day-ahead purchasing price from the grid is shown in Table 2. The

day-in purchasing and selling price to the grid was 1.5 RMB/kWh and 0.2 RMB/kWh [12]. The behavioral parameters of each prosumer were derived from [34].

Table 2. Day-ahead purchasing price from the grid.

Period	Price (RMB/kWh)
10:00–15:00, 18:00–21:00	1.322
7:00–10:00, 15:00–18:00, 21:00–23:00	0.832
23:00–7:00	0.369

The relaxation factor α was set to be 0.8, the quadratic penalty factor ρ was set to 0.002, and the convergence threshold ε was 0.1. In addition, the commercial optimization solver CPLEX12.9 was used to solve the model on the MATLAB 2020a simulation platform.

6.2. Comparison of System Security Performance in Different Schemes

In order to verify the effect of power flow constraints on the security performance, this section compared the system voltage change under the proposed model considering the power flow constraints and the model without considering the power flow constraints [11]. The results are shown in Figure 2. The safe range of system voltage was set as [0.93,1.07], and the results in Figure 2 were the lowest per unit voltage in the system at each time. As can be seen from the Figure 2, there were voltage exceedances from 9:00 to 10:00 and 17:00 to 23:00 under the model without considering power flow constraints, which was due to the high load and low PV output at these periods. Under the model in this paper, ETSP can guide the load reduction and effectively ensure that the voltage at all times is within the safe range by optimizing the purchasing and selling power with prosumers considering power flow constraints.

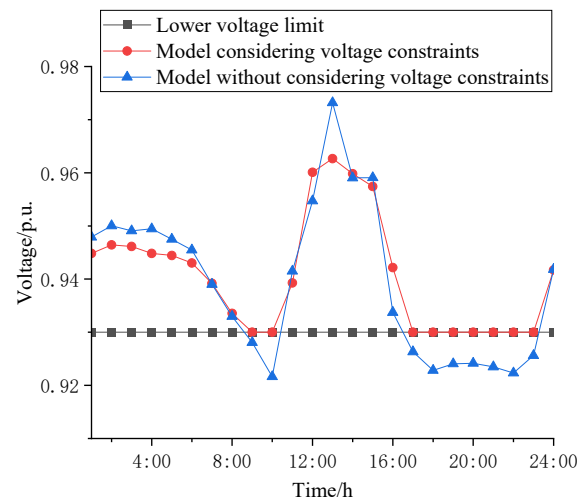


Figure 2. Comparison of system voltage in different cases.

6.3. Operating Characteristic Analysis

6.3.1. External Characteristic Analysis

This section analyzes the purchasing and selling power characteristics presented by the system under P2P transactions. Figure 3 shows the purchasing and selling power of the system from the main grid under the strategy with P2P transactions and the strategy without P2P transactions. Table 3 shows the incomes of ETSP in different cases. It is worth mentioning that in the nonP2P trading case, indirect P2P trading guided by centralized matching of ETSP was not considered. Therefore, in the nonP2P trading case, the system needed to purchase and sell power to the main grid separately.

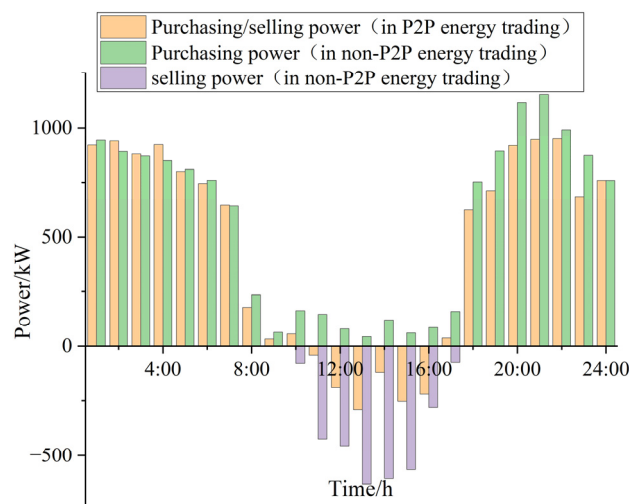


Figure 3. Comparison of purchased/sold power with the main grid in different cases.

Table 3. Income of ETSP in different cases.

Cases	Income/RMB
The strategy within P2P energy market	736.46
The strategy without P2P energy market	482.13

As can be seen from the Figure 3, during the peak hours of PV output from 11:00 to 16:00, P2P transactions within the community were given priority among prosumers, which improved the consumption rate of local PV, so that the power sold by the system to the main grid under the strategy in this paper was significantly lower than that of the case without P2P transactions. In the peak hours of 18:00 to 21:00, the purchasing price was higher and ETSP guided the prosumers to reduce the load. Between the hours of 0:00 to 07:00, the purchasing price was lower and the power consumption was relatively higher in order to meet the overall load demand constraints. Overall, P2P transactions effectively reduced the system's dependence on the purchasing and selling power with the main grid. Accordingly, ETSP can obtain higher returns by optimizing the scheduling of their own energy system to store energy at lower prices and sell energy at higher prices.

6.3.2. Operation Cost Comparison

In order to verify the effectiveness of the strategy proposed in this paper, this section compares the proposed strategy with the traditional stochastic optimization method [19] in terms of power consumption costs, and the results are shown in Table 4. It is worth mentioning that the day-in cost calculated in the traditional stochastic optimization strategy was used as the day-in reference cost, so the day-in prospect value in the traditional stochastic optimization was zero. In addition, this section adopted the 200 scenarios randomly generated as the actual value to verify, and calculated its weighted average to obtain the actual day-in cost.

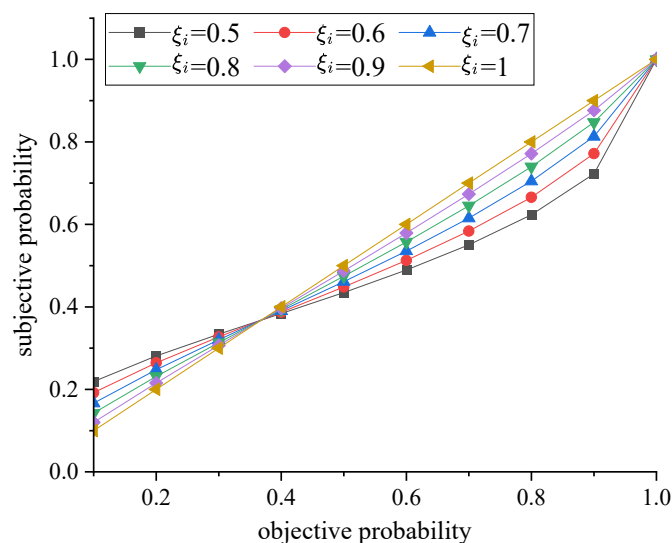
Table 4. Cost comparison of prosumers under different strategies.

		Prosumer 1	Prosumer 2	Prosumer 3	Prosumer 4	Prosumer 5
The proposed strategy	Day-ahead cost/RMB	852.89	969.17	1758.95	618.97	620.65
	Day-in prospect	0.805	2.655	2.961	0.865	0.746
	Actual day-in cost/RMB	56.61	53.82	63.74	36.69	68.36
	Total cost/RMB	909.51	1022.99	1842.69	655.67	689.01
Traditional random optimization	Day-ahead cost/RMB	846.64	943.49	1724.85	612.99	608.23
	Day-in prospect	0	0	0	0	0
	Actual day-in cost/RMB	77.53	99.93	128.72	59.89	86.99
	Total cost/RMB	924.24	1043.43	1853.57	672.88	695.22

In Table 4, due to the fact that the day-in prospect value of the prosumers was introduced under the strategy of this paper, the probability value of the scenario with low probability was overestimated, and the sensitive value of loss was higher than that of profit. Considering that the probability value of adverse scenario was generally small, the weight of adverse scenario under this proposed strategy was increased, resulting in an increase in day-ahead reserve capacity and day-ahead cost. However, the actual day-in cost was significantly reduced compared with traditional stochastic optimization, and the day-in comprehensive prospect was improved, which meant that it was more in line with the psychological characteristics and more accurate at describing the behavior of prosumers. Overall, because the cost coefficients of day-ahead scheduling were lower than that of day-in scheduling, the total cost was lower than that of traditional stochastic optimization.

6.3.3. Operation Cost Comparison

The decision weight coefficient ξ_i determines the psychological evaluation of the difference probability value of prosumers in different scenarios. Figure 4 shows the change of the subjective probability with the true (objective) probability of the event occurring when ξ_i fluctuates in range of the [0.5,1]. As can be seen from the Figure 4, this function will overestimate the probability value of small probability events and reduce the probability value of large probability events. The smaller the coefficient, the stronger the subjectivity of decision makers, showing a state of limited rationality.

**Figure 4.** Decision weight function schematic.

Taking Prosumer 1 as an example, Figures 5 and 6 show the day-ahead cost, day-in prospect and day-in expected costs when ξ_i fluctuates in range of the [0.5,1]. The objective probability of each scenario was [0.0653,0.51, 0.0714,0.1429,0.2104], in which Scenario 1 was the worst scenario, and the net load powers of Scenarios 1, 3, 4, and 5 were higher than the predicted power, and the net load power of Scenario 2 was lower than the predicted power.

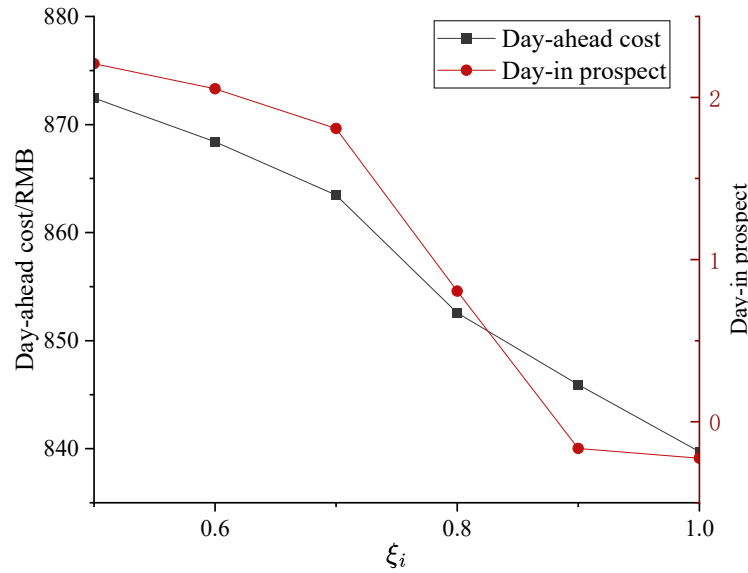


Figure 5. Day-ahead cost and day-in prospect with different ξ_i .

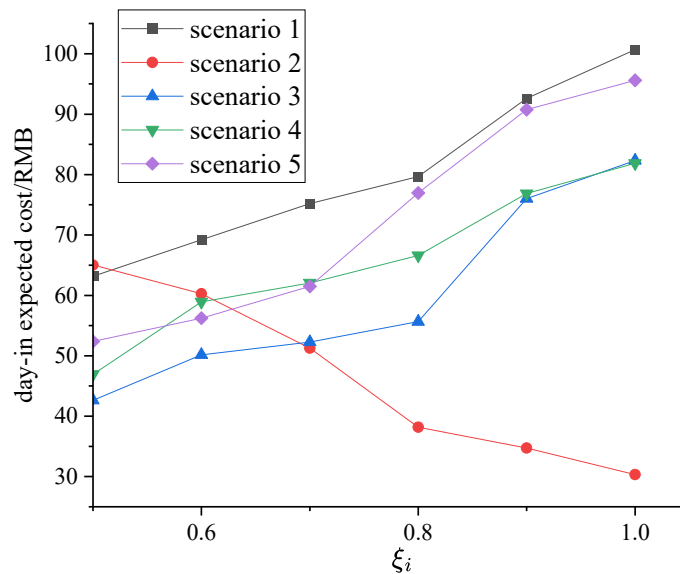


Figure 6. Day-in expected cost of each scenario with different ξ_i .

As can be seen from Figure 4, when the objective probability is greater than 0.4, the prosumer will underestimate the true probability of the event, meaning that its subjective probability will be lower than the objective probability. Therefore, when ξ_i is reduced, the subjective probability of Scenario 2 will gradually decrease, the day-ahead downstream standby capacity will decrease, and its day-in expected cost will gradually increase; this was the worst scenario with a small probability. When the probability of Scenario 1 gradually increases, the up-front spare capacity will also gradually increase. Therefore, the day-in comprehensive prospect will gradually increase, and the day-in expected cost will gradually decrease. Considering that the upward unit reserve cost is higher than the downward unit reserve cost, its day-ahead cost will gradually increase.

6.4. Convergence Analysis

In this paper, the tolerance time of the improved R-ADMM algorithm was set to 500 ms. Figure 7 shows the comparison of algorithm convergence process under the proposed algorithm, R-ADMM algorithm without correction mechanism, and the standard ADMM algorithm. Due to the fact that the update of calculated variables after each iteration through relaxation factor can be controlled to prevent the divergence of iteration process caused by excessive fluctuations in the result, convergence speed can be improved. It can be seen from the Figure 7 that the number of iterations of R-ADMM after the introduction of relaxation factor was significantly lower than that of standard ADMM. In addition, when the agent has an iteration timeout, the agent can still use the predicted boundary information to update the Lagrange multiplier, so the R-ADMM with correction mechanism proposed in this paper has a more accurate information iteration process than the R-ADMM without the correction mechanism. Therefore, the number of iterations was reduced by 11 times, and the total iteration time was reduced by 6.19 s. The stagnation of the convergence process caused by missing boundary variables was avoided, and the convergence speed was accelerated.

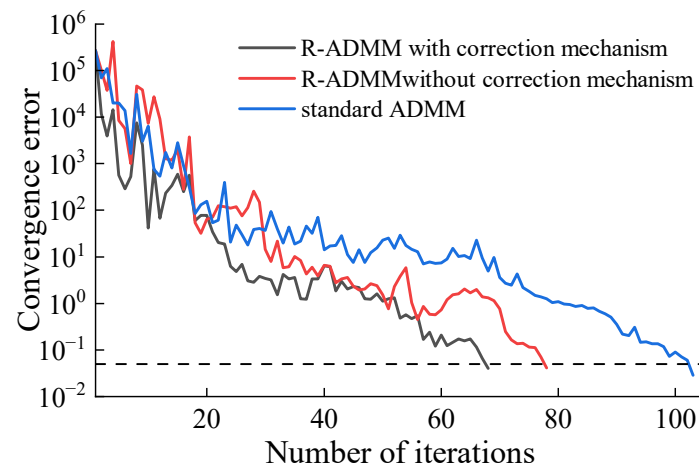


Figure 7. Algorithm convergence process comparison.

Different values of α were set to analyze the effect on evolution of convergence errors. As shown in the Figure 8, the iteration times of the improved R-ADMM algorithm were all smaller than that of the standard ADMM algorithm. When α was larger than 0.5, the number of iterations decreased significantly. With the increase of α , the number of iterations gradually decreased. However, when α was 0.9, the number of iterations increased slightly. Therefore, α was suggested to be selected within [0.7,0.9] and the convergence performance can be improved.

Larger-scale systems consisting of 5 to 30 prosumers were simulated to analyze the scalability of the proposed algorithm. Table 5 shows that the number of iterations and time cost increased with the increasing number of prosumers in the system. Considering that there were usually no more than 30 buildings in a general regional market under the jurisdiction of ETSP [37] and that the simulated maximum consumption time was acceptable for day-ahead energy optimal, the proposed method can be implementable.

Table 5. No. iterations and time cost with different numbers of prosumers.

	5	10	15	20	25	30
No. iterations	67	71	75	82	83	85
time cost/s	61.45	90.11	102.17	129.69	155.22	189.12

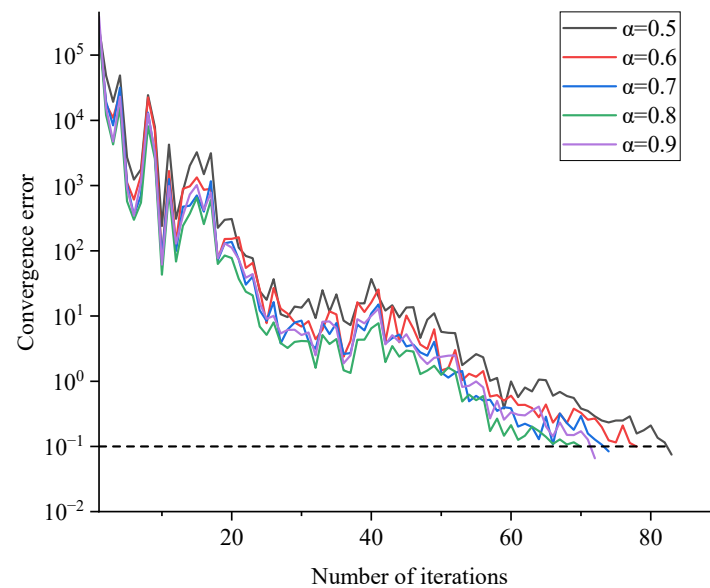


Figure 8. Effect on evolution of convergence errors for different values of α .

7. Conclusions

A P2P transaction optimization operation strategy of prosumers considering bounded rationality was constructed and the following conclusions were obtained through simulated examples:

- (1) Considering the global power flow safety constraints on the ETSP side, a benefit maximization model was constructed to effectively ensure the safety and stability of the system voltage and avoid voltage overruns.
- (2) By introducing prospect theory to convert objective probability into subjective probability of prosumers under bounded rationality, a two-stage energy management stochastic optimization model for prosumers considering P2P transaction and bounded rationality was constructed, which can effectively reduce the comprehensive energy consumption cost of prosumers, improve the comprehensive prospect, and more accurately describe the decision-making behavior of prosumers under bounded rationality.
- (3) Introducing a momentum extrapolation correction mechanism, the proposed improved R-ADMM algorithm can avoid a long convergence time that is too long caused by iteration timeout and improve convergence speed effectively.

It should be mentioned that the algorithm parameter settings were adjusted via simulation experience, and the energy efficiency coefficient and the false data declared by market entities was ignored. Therefore, future work will focus on the parameter adaptive adjustment and benefit maximization under incomplete information to improve the efficiency of energy consumption and the reliability of market transactions.

Author Contributions: Conceptualization, J.H. and Y.S.; methodology, T.H.; software, T.H.; validation, T.H.; formal analysis, T.H.; investigation, J.H. and Y.S.; resources, X.Z.; data curation, Y.Z. and P.W.; writing—original draft preparation, T.H.; writing—review and editing, J.H. and Y.S.; visualization, J.H. and Y.S.; supervision, J.H. and Y.S.; project administration, X.Z.; funding acquisition, X.Z., Y.Z. and P.W. All authors have read and agreed to the published version of the manuscript.

Funding: This research was funded by the state grid corporation of China, grant number 5400-202321242A-1-1-ZN.

Data Availability Statement: The data presented in this study are available on request from the corresponding author.

Conflicts of Interest: Author Xiangpeng Zhan was employed by the Marketing Service Center, State Grid Fujian Electric Power Co., Ltd. Authors Yu Zhang and Peng Wu were employed by the State Grid Energy Research Institute Co., Ltd. The remaining authors declare that the research was

conducted in the absence of any commercial or financial relationships that could be construed as a potential conflict of interest.

Appendix A

As the day-in prospect model (12) was a nonlinear programming, the piecewise linearization method was adopted to transform it into a linear model.

First, the piecewise nonlinear function can be converted to a single function:

$$TDVF_{\omega,i} = u_{\omega,i}^P \cdot (\Delta U_{\omega,i})^{\alpha_i} \delta_i (1 - (1 - \theta_i)r_i)^{1/(1-\theta_i)} + u_{\omega,i}^N \cdot (-\lambda_i(-\Delta U_{\omega,i})^{\beta_i} \delta_i (1 - (1 - \theta_i)r_i)^{1/(1-\theta_i)}) \tag{A1}$$

$$\begin{cases} -M(1 - u_{\omega,i}^P) \leq \Delta U_{\omega,i} \leq u_{\omega,i}^P M \\ -Mu_{\omega,i}^N \leq \Delta U_{\omega,i} \leq M(1 - u_{\omega,i}^N) \\ u_{\omega,i}^P + u_{\omega,i}^N \leq 1 \end{cases} \tag{A2}$$

where M is a positive big number, and the $u_{\omega,i}^P$ and $u_{\omega,i}^N$ are the binary variables.

Then, substitute the $(\Delta C_{\omega,i})^{\alpha_i}$ and the $(-\Delta C_{\omega,i})^{\beta_i}$ by $\sum_{L=1}^{N_L} F_{l,i}^P \varphi_{l,\omega,i}^P$ and $\sum_{L=1}^{N_L} F_{l,i}^N \varphi_{l,\omega,i}^N$ respectively, and a new form of (A1) can be obtained as follows:

$$TDVF_{\omega,i} = u_{\omega,i}^P \cdot \left(\sum_{L=1}^{N_L} F_{l,i}^P \varphi_{l,\omega,i}^P \right) \delta_i (1 - (1 - \theta_i)r_i)^{1/(1-\theta_i)} + u_{\omega,i}^N \cdot \left(-\lambda_i \left(\sum_{L=1}^{N_L} F_{l,i}^N \varphi_{l,\omega,i}^N \right) \delta_i (1 - (1 - \theta_i)r_i)^{1/(1-\theta_i)} \right) \tag{A3}$$

$$-u_{\omega,i}^N M \leq \Delta C_{\omega,i} - \sum_{L=1}^{N_L} \varphi_{l,\omega,i}^P \leq M(1 - u_{\omega,i}^P) \tag{A4}$$

$$-u_{\omega,i}^P M \leq \Delta C_{\omega,i} - \sum_{L=1}^{N_L} \varphi_{l,\omega,i}^N \leq M(1 - u_{\omega,i}^N) \tag{A5}$$

$$0 \leq \sum_{L=1}^{N_L} F_{l,i}^P \varphi_{l,\omega,i}^P \leq Mu_{\omega,i}^P \tag{A6}$$

$$0 \leq \sum_{L=1}^{N_L} F_{l,i}^N \varphi_{l,\omega,i}^N \leq Mu_{\omega,i}^N \tag{A7}$$

$$\varphi_{l,\omega,i}^{P_min} \leq \varphi_{l,\omega,i}^P \leq \varphi_{l,\omega,i}^{P_max} \tag{A8}$$

$$\varphi_{l,\omega,i}^{N_min} \leq \varphi_{l,\omega,i}^N \leq \varphi_{l,\omega,i}^{N_max} \tag{A9}$$

where N_L is the number of segments, $F_{l,i}^P$ and $\varphi_{l,i}^P$ are the slope and equivalent spacing of $(\Delta C_{\omega,i})^{\alpha_i}$ respectively, $F_{l,i}^N$ and $\varphi_{l,\omega,i}^N$ are the slope and equivalent spacing of $(-\Delta C_{\omega,i})^{\beta_i}$ respectively.

Since (A3) is still a nonlinear function, it is further transformed by piecewise linearization, and the following linear model can be obtained:

$$TDVF_{\omega,i} = \zeta_{\omega,i}^P \cdot \delta_i (1 - (1 - \theta_i)r_i)^{1/(1-\theta_i)} + \zeta_{\omega,i}^N \cdot (-\lambda_i \delta_i (1 - (1 - \theta_i)r_i)^{1/(1-\theta_i)}) \tag{A10}$$

$$\sum_{L=1}^{N_L} F_{l,i}^P \varphi_{l,\omega,i}^P - (1 - u_{\omega,i}^P)M \leq \zeta_{\omega,i}^P \leq u_{\omega,i}^P M \tag{A11}$$

$$0 \leq \zeta_{\omega,i}^P \leq \sum_{L=1}^{N_L} F_{l,i}^P \varphi_{l,\omega,i}^P \quad (\text{A12})$$

$$\sum_{L=1}^{N_L} F_{l,i}^N \varphi_{l,\omega,i}^N - (1 - u_{\omega,i}^N)M \leq \zeta_{\omega,i}^N \leq u_{\omega,i}^N M \quad (\text{A13})$$

$$0 \leq \zeta_{\omega,i}^N \leq \sum_{L=1}^{N_L} F_{l,i}^N \varphi_{l,\omega,i}^N \quad (\text{A14})$$

Appendix B

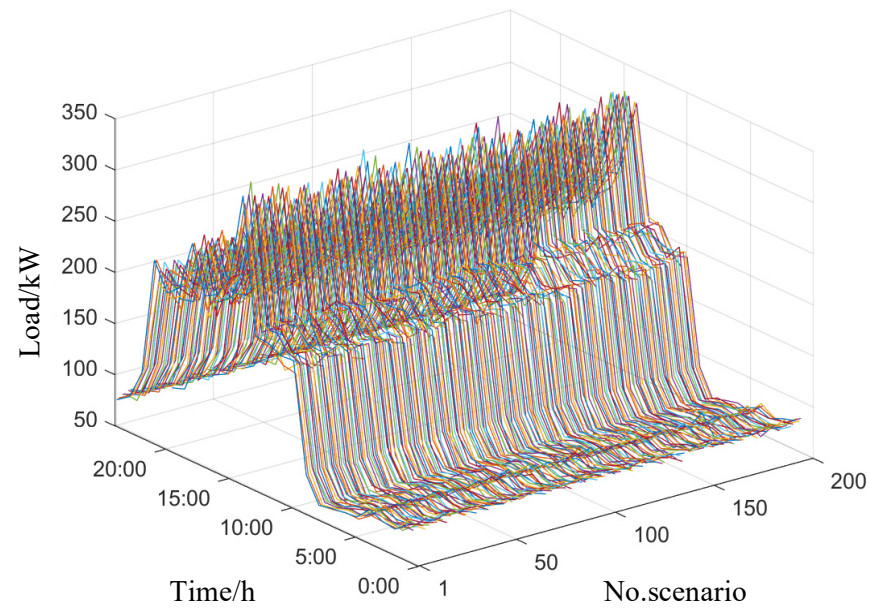


Figure A1. Different power load curves generated in 200 scenarios.

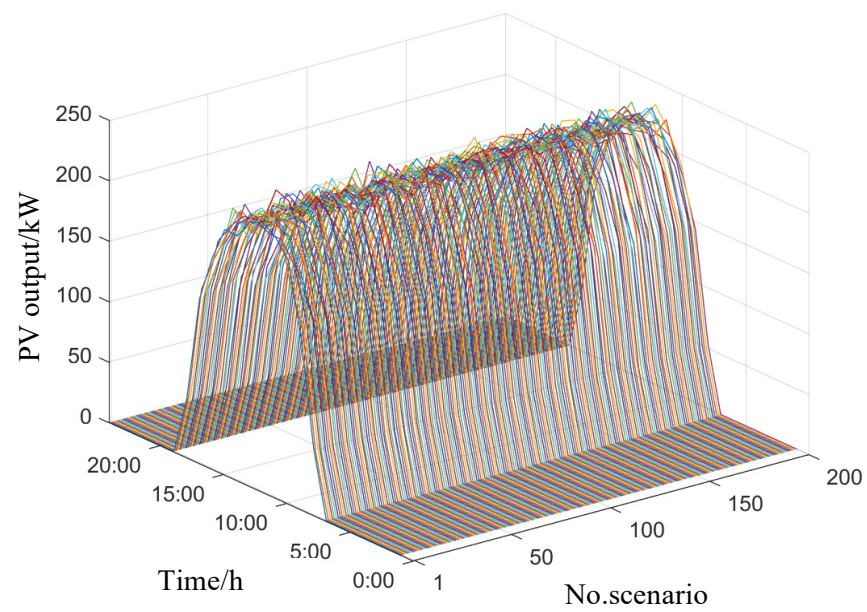


Figure A2. Different PV output curves generated in 200 scenarios.

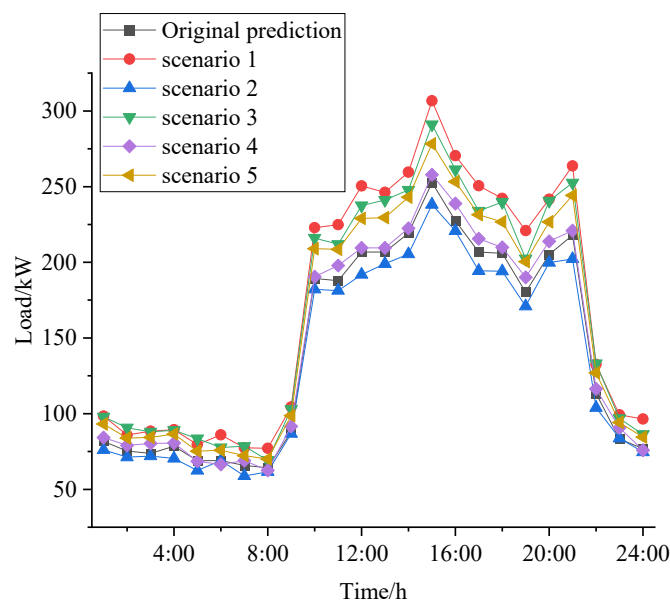


Figure A3. Scenario of the reduction in load power.

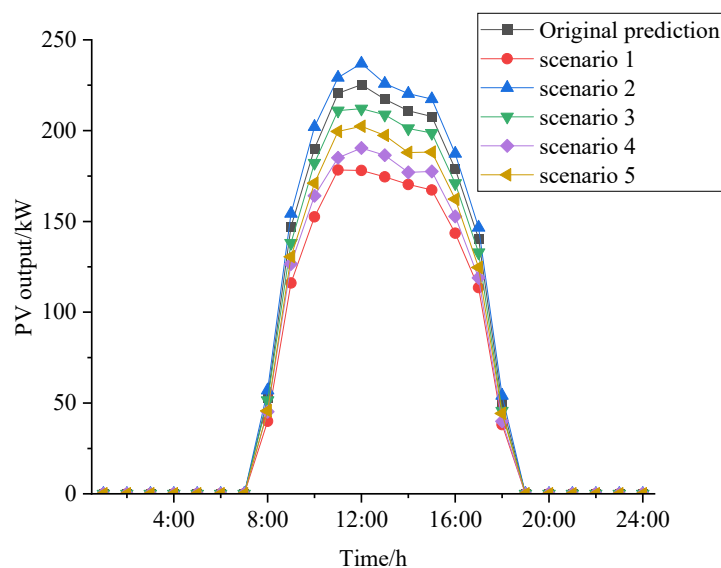


Figure A4. Scenario of the reduction in PV output.

References

1. Walter, L.F.; Lais, V.T.; Amanda, L.S.; Janaina, M.; Thais, D.; Salvador, R.D.M.; Elvira, F.B.; Joao, H.P.P.E.; Ayyoob, S.; Maria, A.; et al. Prosumers and sustainable development: An international assessment in the field of renewable energy. *Sustain. Futures* **2024**, *7*, 100158.
2. Wang, X.; Jia, H.; Jin, X.; Mu, Y.; Yu, X.; Liang, S. Bi-level optimal operations for grid operator and low-carbon building prosumers with peer-to-peer energy sharing. *Appl. Energy* **2024**, *359*, 122723. [[CrossRef](#)]
3. Lee, M.; Han, C.; Kwon, S.; Kim, Y. Energy and cost savings through heat trading between two massive prosumers using solar and ground energy systems connected to district heating networks. *Energy* **2023**, *284*, 129347. [[CrossRef](#)]
4. David, F.; Mark, K.; Ron, M. The view from the top of the mountain: Building a community of practice with the gridwise transactive energy framework. *IEEE Power Energy* **2016**, *12*, 25–33.
5. Xia, Y.; Xu, Q.; Chen, L.; Du, P. The flexible roles of distributed energy storages in peer-to-peer transactive energy market: A state-of-the-art review. *Appl. Energy* **2022**, *327*, 120085. [[CrossRef](#)]
6. Yan, X.; Song, M.; Cao, J.; Gao, C.; Jing, X.; Xia, S.; Ban, M. Peer-to-Peer transactive energy trading of multiple microgrids considering renewable energy uncertainty. *Int. J. Electr. Power Energy Syst.* **2023**, *152*, 109235. [[CrossRef](#)]
7. Lucas, S.M.; Fernando, L.T.; Diego, I.; Marcos, E.P.M.; Giovanni, C.B.; Raimundo, F.S.; Ruth, P.S.L. Co-simulation platform for the assessment of transactive energy systems. *Electr. Power Syst. Res.* **2023**, *223*, 109693.

8. Dylan, C.; Ted, K.; Sivasathya, B.; Tarek, E.; Siddharth, S.; Jeff, M.; Dane, C. Co-simulation of transactive energy markets: A framework for market testing and evaluation. *Int. J. Electr. Power Energy Syst.* **2021**, *128*, 106664.
9. Abba, L.B.; Mukhtar, F.H.; Sara, A.; Abobaker, K.A.; Babangida, M.; Soheil, M.; Alan, C.B.; Chukwama, O.; Kunduli, M.; Harrison, O.I. Peer-to-peer electricity trading: A systematic review on current developments and perspectives. *Renew. Energy Focus* **2023**, *44*, 317–333.
10. Boumaiza, A. A Blockchain-based scalability solution with microgrids peer-to-peer trade. *Energies* **2024**, *17*, 915. [[CrossRef](#)]
11. Huang, T.; Sun, Y.; Hao, J.; Sun, C.; Liu, C. A distributed peer-to-peer energy trading model in integrated electric-thermal system. *IET Renew. Power Gener.* **2023**, 1–16. [[CrossRef](#)]
12. Md, H.U.; Jae, D.P. Peer-to-peer energy trading in transactive markets considering physical network constraints. *IEEE Trans. Smart Grid* **2021**, *12*, 3390–3403.
13. Wang, Z.; Yu, X.; Mu, Y.; Jia, H.; Jiang, Q.; Wang, X. Peer-to-Peer energy trading strategy for energy balance service provider (EBSP) considering market elasticity in community microgrid. *Appl. Energy* **2021**, *303*, 117596. [[CrossRef](#)]
14. Meysam, K.; Pedro, F.; Zita, V. A distributed robust ADMM-based model for the energy management in local energy communities. *Sustain. Energy Grids* **2023**, *36*, 101136.
15. Seyed, M.H.; Raffaele, C.; Alessandra, P.; Mariagrazia, D. Robust Decentralized Charge Control of Electric Vehicles under Uncertainty on Inelastic Demand and Energy Pricing. In Proceedings of the IEEE International Conference on Systems, Man, and Cybernetics (SMC) 2020, Toronto, ON, Canada, 11–14 October 2020; pp. 1834–1839.
16. Zhang, Y.; Zhao, H.; Li, B. Distributionally robust comprehensive declaration strategy of virtual power plant participating in the power market considering flexible ramping product and uncertainties. *Appl. Energy* **2023**, *343*, 121133.
17. Chang, Y.; Zheng, L. Distributed Conditional-Distributionally robust coordination for an electrical power and flexibility-enhanced district heating system. *Appl. Energy* **2023**, *347*, 121491.
18. Jayachandranath, J.; Debapriya, D. Stochastic planning of islanded microgrids with uncertain multi-energy demands and renewable generations. *IET Renew. Power Gener.* **2020**, *14*, 4179–4192. [[CrossRef](#)]
19. Zhang, Z.; Yao, J.; Zheng, R. Multi-Objective optimization of building energy saving based on the randomness of energy-related occupant behavior. *Sustainability* **2024**, *16*, 1935. [[CrossRef](#)]
20. Kreishan, M.Z.; Zobaa, A.F. Scenario-Based uncertainty modeling for power management in islanded microgrid using the mixed-integer distributed ant colony optimization. *Energies* **2023**, *16*, 4257. [[CrossRef](#)]
21. Hasan, E.; Sadjad, G.; Vahid, T.; Mohammad, F.K. A conditional value at risk based stochastic allocation of SOP in distribution networks. *Electr. Power Syst. Res.* **2024**, *228*, 110111.
22. Liu, Z.; Li, C. Low-Carbon Economic Optimization of Integrated Energy System Considering Refined Utilization of Hydrogen Energy and Generalized Energy Storage. *Energies* **2023**, *16*, 5700. [[CrossRef](#)]
23. Yao, Y.; Gao, C.; Chen, T.; Yang, J.; Chen, S. Distributed electric energy trading model and strategy analysis based on prospect theory. *Int. J. Electr. Power Energy Syst.* **2021**, *132*, 106865. [[CrossRef](#)]
24. Wang, J.D.; Xu, Q.M.; Su, H.L.; Fang, K.J. A distributed and robust optimal scheduling model for an active distribution network with load aggregators. *Front. Energy Res.* **2021**, *9*, 646869. [[CrossRef](#)]
25. Wang, J.; Li, L.; Jiangfeng, Z. Deep reinforcement learning for energy trading and load scheduling in residential peer-to-peer energy trading market. *Int. J. Electr. Power Energy Syst.* **2023**, *147*, 108885. [[CrossRef](#)]
26. Dawei, Q.; Yujian, Y.; Dimitrios, P.; Goran, S. Scalable coordinated management of peer-to-peer energy trading: A multi-cluster deep reinforcement learning approach. *Appl. Energy* **2021**, *292*, 116940.
27. Chen, Z.; Li, Z.; Guo, C.; Wang, J.; Ding, Y. Fully distributed robust reserve scheduling for coupled transmission and distribution systems. *IEEE Trans. Power Syst.* **2021**, *36*, 169–182. [[CrossRef](#)]
28. Peiling, C.; Yujian, Y.; Hongru, W.; Siqi, B.; Yi, T.; Goran, S. Holistic coordination of transactive energy and carbon emission right trading for heterogenous networked multi-energy microgrids: A fully distributed adaptive consensus ADMM approach. *Sustain. Energy Technol. Assess.* **2024**, *64*, 13729.
29. Seyed, M.H.; Raffaele, C.; Jan, J.; Mariagrazia, D. Multi-block ADMM Approach for Decentralized Demand Response of Energy Communities with Flexible Loads and Shared Energy Storage System. In Proceedings of the 30th Mediterranean Conference on Control and Automation (MED) 2022, Athens, Greece, 28 June–1 July 2022; pp. 67–72.
30. Qing, Y.; Hao, W. Distributed energy trading management for renewable prosumers with HVAC and energy storage. *Energy Rep.* **2021**, *7*, 2512–2525.
31. Li, W.; Qian, T.; Zhao, W.; Huang, W.C.; Zhang, Y.; Xie, X.; Tang, W. Decentralized optimization for integrated electricity–heat systems with data center based energy hub considering communication packet loss. *Appl. Energy* **2023**, *350*, 121586. [[CrossRef](#)]
32. Tang, W.; Zhao, W.; Qian, T.; Zhao, B.; Lin, Z.; Xin, Y. Learning-accelerated asynchronous decentralized optimization for integrated transmission and distribution systems over lossy networks. *Sustain. Energy Grids* **2022**, *31*, 100724. [[CrossRef](#)]
33. Jess, B.; Alberto, B.; Andrew, S. Present-bias, quasi-hyperbolic discounting, and fixed costs. *Game Econ. Behav.* **2010**, *69*, 205–223.
34. Sobhan, D.; Masoud, R.; Seyed, F.F.A.; Amir, A.; Mohammad, R.S. A Peer-to-Peer energy trading market model based on time-driven prospect theory in a smart and sustainable energy community. *Sustain. Energy Grids* **2021**, *28*, 100542.
35. Bolognani, S.; Zampieri, S. On the existence and linear approximation of the power flow solution in power distribution networks. *IEEE Trans. Power Syst.* **2016**, *31*, 163–172. [[CrossRef](#)]

36. Jing, R.; Xie, M.; Wang, X.; Chen, L. Fair P2P energy trading between residential and commercial multi-energy systems enabling integrated demand-side management. *Appl. Energy* **2020**, *262*, 114551. [[CrossRef](#)]
37. Chen, L.D.; Liu, N.; Li, C.C.; Wang, J.H. Peer-to-peer energy sharing with social attributes: A stochastic leader-follower game approach. *IEEE Trans. Ind. Inform.* **2021**, *17*, 1545–1556. [[CrossRef](#)]

Disclaimer/Publisher’s Note: The statements, opinions and data contained in all publications are solely those of the individual author(s) and contributor(s) and not of MDPI and/or the editor(s). MDPI and/or the editor(s) disclaim responsibility for any injury to people or property resulting from any ideas, methods, instructions or products referred to in the content.